Micro Cameras Capable of Multiple Viewpoint Imaging Utilizing Photoresist Microlens Arrays

Bader Aldalali, Chenhui Li, Li Zhang, and Hongrui Jiang, *Senior Member, IEEE*

***Abstract*—We present micro cameras that provide multiple viewpoint imaging from one single image capture and without moving the camera. The micro cameras are based on lightfield photography where the camera captures the 4-D lightfield and images it onto a 2-D charge-coupled device (CCD) sensor through the use of a microlens array. The microlens array was fabricated using the photoresist reflow process. Two micro cameras were realized. One camera has a 15.2-mm aperture, a 97 × 97 microlens array of 230-μm pitch size, and a 1-megapixel CCD and is capable of 100 different viewpoints with a viewing angle of approximately 20°. The other camera has a 9-mm aperture, a 56 × 42 microlens array of 80-μm pitch size, and a 5-megapixel CCD and is capable of around 1000 different viewpoints with a viewing angle of approximately 4.7°. The resolution of the images rendered from the two cameras is 97 × 97 and 56 × 42 pixels, respectively. [2011-0314]**

***Index Terms*—Lightfield, micro camera, microlens array, multiple viewpoints, plenoptic camera.**

I. Introduction

MICRO CAMERAS are typically fixed in place or used in environments with limited space for maneuverability. In endoscopy, for example, obstructing objects that block the line of sight of the intended object requires maneuvering of the endoscope around the obstruction and performing multiple tries in order to achieve the right viewpoint. This maneuverability is hard and sometimes impossible [1]. Such hardship in maneuverability lies in the generally limited space to place, adjust, and perform other operations of the cameras. These issues could potentially be addressed by introducing the concept of plenoptic cameras to form microscale cameras that can work in such environments.

On the macroscale, a plenoptic camera is one that utilizes an embedded microlens array to capture a single image which contains much richer information than that captured from a conventional camera [2]. This information, referred to as the lightfield, can subsequently be digitally processed to produce synthetic images as if seen from different viewpoints. In free space, the lightfield is a 4-D function describing the intensity of light in terms of *both* position *and* direction [3]. To capture the lightfield, a microlens array must be placed at a certain position in the camera. Without the microlens array, as in a conventional camera, the lightfield cannot be captured because the light impinging on the camera lens(es) from all different directions is averaged onto the sensor pixels of the camera. All information regarding the direction of the impinging light is thereby lost.

The concept of lightfield capture, which is better known as lightfield photography, dates back to Lipmann and his idea of integral photography [4]. In 1908, he placed an array of small lenses on top of a film plate to image 3-D information onto a 2-D surface. However, due to the nonexistence of digital photography at that time, the concept could not be explored further [4], [5]. There are different approaches for capturing the lightfield that have evolved over time [6]–[12], with two common features among all of these approaches. The first is that they all share the same goal of capturing information relating to the position and direction of the incoming light. Another common feature is that they are all based on macroscale cameras for use in macroscale environments. Here, our approach is to use the idea of plenoptic cameras and apply it at the microscale. Within the realm of micro cameras, there are existing cameras that employ similar approaches. For example, Fife *et al.* reported a multiaperture image sensor which offers higher spatial resolution at the expense of diminished angular resolution, which limits the capability of multiple view [13]. In another approach, an endoscope was realized that provides two optical paths to realize stereo vision but provides no multiple-view capability [14].

We report on two micro cameras that are capable of multiple viewpoint imaging from a single image capture, utilizing photoresist microlens arrays. Preliminary results were reported by our group in [15]. Here, we present expanded work on the design, realization, and characterization of the micro cameras and report on higher performance in terms of multiple viewpoint capability. We achieved 100 and approximately 1000 different viewpoints for the two cameras with viewing angles of approximately 20° and 4.7°, respectively, which offer better results than those in [13] and [14]. Aberration measurements of different shapes of photoresist microlenses with their effect on the image quality of the camera are also presented. It should be noted that plenoptic cameras can also synthesize images that are

Manuscript received October 25, 2011; revised March 14, 2012; accepted March 27, 2012. Date of publication May 4, 2012; date of current version July 27, 2012. This work was supported by the U.S. National Science Foundation through the Emerging Frontiers in Research and Innovation program under Grant EFRI 09737847. The work of B. Aldalali was supported by Kuwait University through the graduate student scholarship program. Subject Editor O. Solgaard.

B. Aldalali and C. Li are with the Department of Electrical and Computer Engineering, University of Wisconsin, Madison, WI 53706 USA (e-mail: aldalali@wisc.edu; cli26@wisc.edu).

L. Zhang is with the Department of Computer Sciences, the Department of Electrical and Computer Engineering, and the Eye Research Institute, University of Wisconsin, Madison, WI 53706 USA (e-mail: lizhang@wisc.edu).

H. Jiang is with the Department of Electrical and Computer Engineering, the Materials Science Program, the Department of Biomedical Engineering, and the Eye Research Institute, University of Wisconsin, Madison, WI 53706 USA (e-mail: hongrui@engr.wisc.edu).

Color versions of one or more of the figures in this paper are available online at http://ieeexplore.ieee.org.

Digital Object Identifier 10.1109/JMEMS.2012.2194773

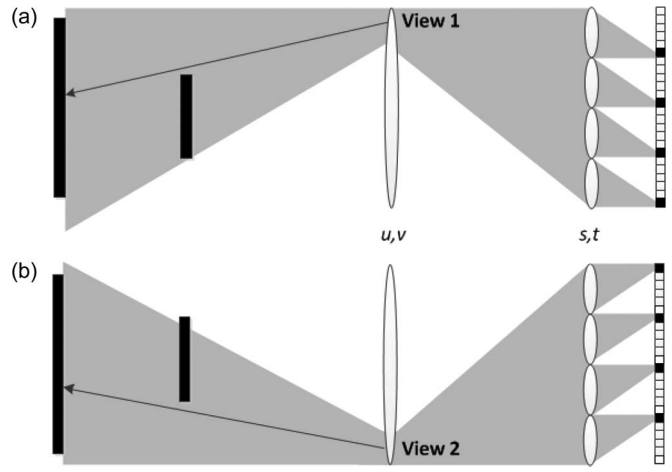

Fig. 1. Schematic of a micro plenoptic camera. In this example setup, there is 6 pixels under each microlens which translates to six different viewpoints. Each viewpoint corresponds to a different subregion of the main lens. (a) No. 1 pixels of all microlenses are imaged by a corresponding subregion of the main lens which only allows light from a distinct viewpoint of Object 2 to pass. (b) Different view of Object 2 is imaged onto No. 6 pixels of all microlenses which correspond to the bottom subregion of the main lens.

refocused to different depths; nevertheless, refocusing is of little significance to us since the depth of field is already extended with a much smaller aperture of the cameras.

II. Principle and Structure

Since the lightfield describes light at any point in space, it can be parameterized in a number of ways [16]. The most common is the Cartesian coordinate two-plane parameterization. The 4-D lightfield $L(u, v, s, t)$ describes the light intersecting two planes (u, v) and (s, t)[3]. In the case of the plenoptic camera, the (u, v) plane refers to the camera aperture plane, while the (s, t) plane refers to the microlens array plane [6]. Fig. 1 shows the schematic of a micro plenoptic camera. The camera consists of a main lens, a microlens array, and a charge-coupled-device (CCD) chip. The microlens array is placed at the image plane of the main lens, and the CCD chip is placed at the focal length of the microlens array where the same number of pixels is under each microlens [2]. The light rays refracted from the main lens are combined in the image plane, as in a regular camera. However, since the microlens array is at the image plane and not the CCD, the light rays further separate and reach distinct pixels behind the microlens array with each pixel representing a distinct direction of the incoming light.

As seen in Fig. 1, the light corresponding to a certain viewpoint of an object passes through a certain subregion of the main lens and is imaged through all the microlenses onto 1 pixel/microlens. The imaging equation governing each pixel exposure, assuming paraxial approximation and a completely open aperture, is given by the following equation [6]:

$$I(s,t) = \iint L(u,v,s,t)dudv. \tag{1}$$

From the aforementioned equation, the pixel exposure is basically an integral of the intensity of light over the entire aperture. The use of the microlens array allows differentiation between the directions of the incoming rays. In terms of the aforementioned equation, to extract an image corresponding to one viewpoint is equivalent to keeping u and v fixed (choosing one subregion) and going over all s and t (all the microlenses). The number of available viewpoints is equal to the number of pixels. This process of digitally choosing the same pixel under each microlens to synthesize the resulting photograph is equivalent to capturing an image from a camera with an aperture equal to the subregion of the main lens and at the same angle.

To achieve the sharpest image possible under each microlens requires matching the f-number of the main lens and the microlens array. The f-number is defined as the ratio of the focal length over the lens aperture and describes the relative aperture of the lens. In this case, we need to match the image-side f-number, which is the image distance over the lens aperture, to the f-number of the microlens array. If the image-side f-number is lower (larger relative aperture) than the microlens array f-number, the images under the microlenses will overlap. If the image-side f-number is higher (smaller relative aperture) than the microlens array f-number, the images under each microlens will not utilize all the available pixels, and there will be dark spots between neighboring microlenses [6].

III. Fabrication

As seen in Fig. 1, the microlens array is an integral part of the plenoptic camera. The microlens array was fabricated using the photoresist thermal reflow method [17]. Photoresist reflow is a very common method used to fabricate refractive microlenses due to its low cost, simplicity, as well as better control [17]. In the reflow method, baking photoresist at a temperature higher than its glass transition temperature melts the photoresist and allows the photoresist molecules to reflow. Due to the surface tension between photoresist and the underlying substrate, reflowing will result in a lens-shaped structure with a focal length dependent on the initial photoresist thickness, reflow time, and temperature. The focal length of the final photoresist microlens array is governed by the thin lens equation

$$f = \frac{R}{n-1} \tag{2}$$

where f is the focal length of the microlens, R is the radius of curvature, and n is the refractive index of the photoresist which is equal to 1.64 [18]. The first micro camera (camera A) that we will show later has a 97 $\times$ 97 microlens array of 230-μm pitch size, a focal length of about 1.2 mm, as well as a 1-megapixel CCD. The second camera (camera B) has a 56 $\times$ 42 microlens array of 80-μm pitch size, a focal length of about 500 μm, as well as a 5-megapixel CCD.

A. Equipment and Materials

Photolithography procedures were carried out using a desktop EXFO Acticure 4000 (EXFO Photonic Solutions, Inc., Mississauga, ON, Canada) ultraviolet (UV) light source. Photomasks for camera A were printed using high-resolution films (3000 dpi, Imagesetter, Inc., Madison, WI, USA). For

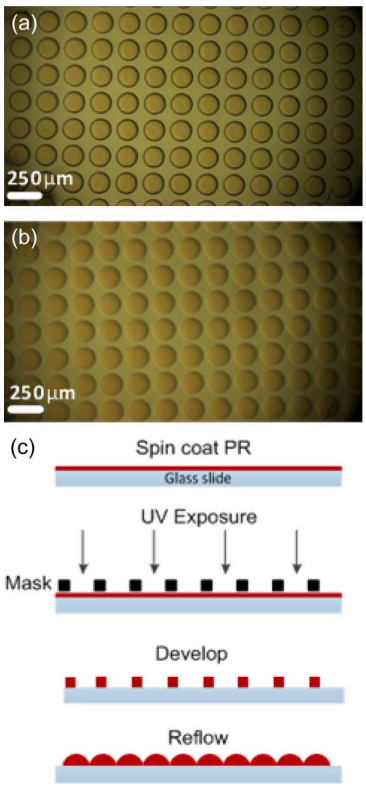

Fig. 2. (a) Microlens array before photoresist reflow. (b) Microlens array after reflow. (c) Fabrication process. The focal length of the microlenses is dependent on the initial thickness of the photoresist, pitch, reflow time, and temperature.

Camera B, photomasks were printed using higher resolution films (Fineline Imaging, Colorado Springs, CO, USA). The photoresist used in fabricating the microlens array was AZ P4620 along with the AZ400K developer (AZ Electronic Materials, Branchburg, NJ, USA).

B. Fabrication Process

The fabrication process of the microlens array for the 1-megapixel and 5-megapixel cameras are essentially the same; the only difference is the time and intensity of the exposure and the development time. For the microlens array used for camera A with 230-μm pitch, AZ P4620 photoresist was spin coated onto a glass substrate and soft baked at 110 °C for 90 s. The substrate was then exposed with UV light at 480 mJ/cm^2, followed by development with 1:4 diluted AZ 400 K developer for 150 s. At 150 s, the photoresist had not fully developed, and there was a thin layer of undeveloped photoresist remaining on the substrate. This thin layer would help the photoresist columns to reflow and increase the microlens array fill factor [16]. Fig. 2(a) shows photoresist columns before reflow. The substrate was then hard baked at 165 °C for 150 s. Fig. 2(b) shows the final microlens array, and Fig. 2(c) shows the process flow.

IV. Experiments and Results

As defined before, we made two experimental micro cameras, A and B, with different CCD pixel resolutions. Both cameras include a main lens, a photoresist microlens array with circular apertures, and a CCD sensor. The choice of circular apertures is related to the aberrations associated with the lens shape which is further studied in the discussion section later.

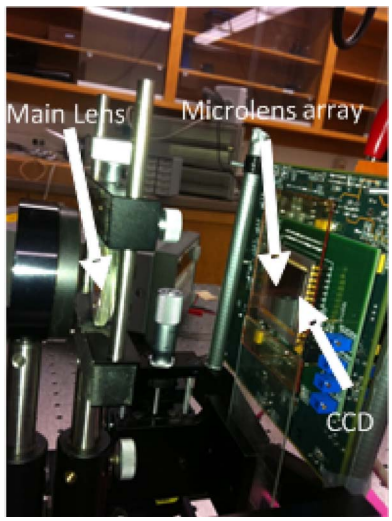

Fig. 3. Experimental setup of our micro camera A showing a main lens (aperture of 15.2 mm; f/2.5), microlens array (97 $\times$ 97; pitch size: 230 μm; focal length: $\sim$1.2 mm), and a 1-megapixel CCD chip.

A. Experimental Micro Camera With 1-Megapixel CCD—Camera A

Fig. 3 shows camera A. We used a 15.2-mm-aperture main lens of approximately f/2.5 and a 97 $\times$ 97 photoresist microlens array of 230-μm pitch size and about 1.2-mm focal length, along with a 1-megapixel board-level CCD having pixel sizes of 24 μm (KAF-1001, Kodak Image Sensor Solutions, Rochester, NY, USA). To ensure that the f-numbers were matched, we observed the lightfield image produced by the camera. As mentioned earlier in Section II, we could deduce from the image whether the f-number of the main lens was larger, matched, or smaller than the microlens array f-number. If the image showed microlenses overlapping each other, then the main lens image-side f-number was smaller than the microlens f-number. If the image showed microlenses surrounded by dark pixels, then the image-side f-number was larger than the microlens f-number. This configuration translates to approximately 10 $\times$ 10 different viewpoints. To confirm, we simulated the setup using the software POV-Ray [19]. Fig. 4 shows simulation results of our experimental setup.

Fig. 5(a) shows the real lightfield image captured using camera A. Using MATLAB, we first resized the captured image such that there were an integer number of pixels under each microlens. We then diced the 2-D image into a 4-D array $L(u, v, s, t)$ where (u, v) chose the pixel and (s, t) chose the microlens. This was possible since the sensor plane is parallel to the microlens array plane. We then digitally chose the same pixel from all the microlenses by choosing the same u or v from all the microlenses, resulting in a synthetic photograph with a resolution equal to the number of microlenses and with a distinctive viewpoint. Using a computer with a quad core processor and 4 GB of random-access memory, the time needed

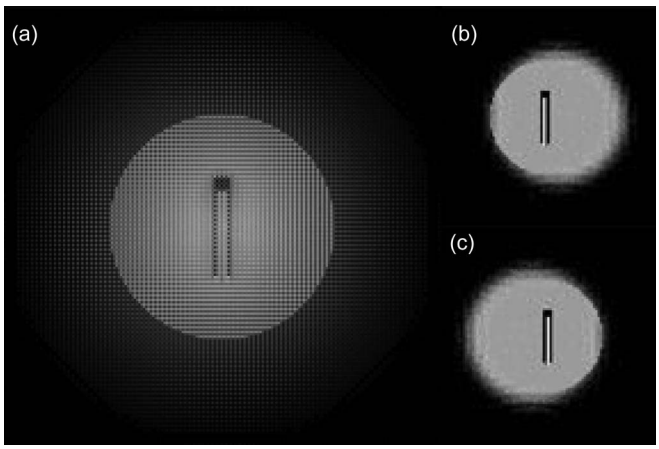

Fig. 4. Simulation result of our micro camera A using a 15.2-mm aperture, f/2.5 main lens, and a 97 $\times$ 97 230-μm-pitch microlens array. (a) Captured lightfield of two objects, one bright line and one dark line. The angle is such that the bright line is blocking the dark line, and thus, only the bright line can be seen. (b) and (c) show the digitally postprocessed images where the dark line can now be seen from varied angles. Had it been a conventional camera, the dark line would not have been shown.

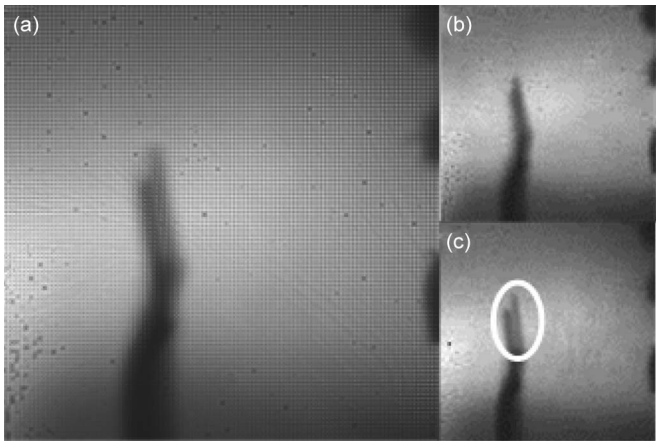

Fig. 5. Experimental results of our micro camera A. (a) Captured lightfield of two wires that are placed along the same axis. (b) and (c) show the digitally postprocessed images where the view of the separation of the wires changes when changing the viewpoint.

to render an image with a distinctive viewpoint was on the order of 100 ms. Fig. 4(b) and (c) shows two of these viewpoints. Fig. 5 shows the results of our experiment. When comparing Figs. 4 and 5, we see that the capability of rendering different viewpoints for camera A matches well with the simulation results. It is worth noting that, as can be seen in Fig. 4 or 5, the resolution of the final synthetic images (97 $\times$ 97) is much smaller than the resolution of the captured lightfield ($\sim$1000 $\times$ 1000).

B. Experimental Micro Camera With 5-Megapixel CCD—Camera B

One of the requirements of the micro camera is to have the CCD imager fixed at the focal length of the microlens array. Due to the limitations of the CCD chip used in camera A, we could only adjust the positions of the microlens array and the CCD chip, based on calculated focal length of the microlenses, to approximately satisfy this requirement. The CCD used in camera A had pixel sizes of 24 μm. This translates to very sensitive pixels, and even low-level lighting in a relatively dark room would saturate the pixels. It was thus impractical for us to adjust the positions of the microlens array and the CCD chip by introducing incoming collimated light before covering the whole setup in a black box to take the images. Another camera, Camera B, was realized to ensure this requirement, as well as to provide a higher number of available viewpoints.

Camera B had a main lens aperture of approximately 9 mm, a focal length of 25 mm, a 56 $\times$ 42 photoresist microlens array with a focal length of 500 μm, and a 5-megapixel board-level CCD having pixel sizes of 2.2 μm (BCN-C050-U, Mightex Systems, Toronto, ON, Canada). The small size of the pixels allowed for lower sensitivity and prevented saturation of the pixels. Therefore, we were able to use collimated light to guide us in placing the CCD at the focal length of the microlens array. We used a collimated light source and placed both the microlens array and the CCD chip on translational stages. Using the micrometer drive of the translational stage, we then moved the microlens array until we could see an array of clear focused spots as the image on the CCD. At this position, the CCD was placed at the focal length of the microlens array. The main lens was then added in front of the microlens array. The only requirement in terms of placement of the main lens was that it had to be in a position where the main lens image-side f-number matched the microlens array f-number. In this case, since we fixed the aperture of the main lens at 9 mm, and the microlens f-number is fixed at $\sim f$/6.25, the main lens was placed a distance of $\sim$56 mm from the microlens array. Fig. 6 shows the experiment results. Fig. 6(a) shows the lightfield image captured by the camera, and Fig. 6(b) shows 47 different viewpoints.

C. Simulation of a 2-mm-Aperture Micro Camera

Due to the fabrication limitation, at this moment, cameras A and B are the smallest that we could achieve. To illustrate the effect of a smaller camera, we also simulated a third micro camera using POV-Ray. The camera has a main lens with a 2-mm aperture, a 69 $\times$ 69 microlens array of 50-μm pitch size, and a 5-megapixel CCD. Fig. 7 shows the simulation results. Fig. 7(a) shows the lightfield image captured by the camera. We then input the captured lightfield to the algorithm mentioned earlier to generate the different synthetic images with distinct viewpoints. Fig. 7(b) and (c) shows two of these viewpoints. In this simulation, there are approximately 72 pixels per microlens or 72 $\times$ 72 different viewpoints.

V. Discussion

A. Spatioangular Resolution Tradeoff

There exists a tradeoff between the number of viewpoints available which is referred to as the angular resolution and the resolution of the final processed image which is referred to as the spatial resolution. The spatial resolution of the micro camera is determined by the number of microlenses, while

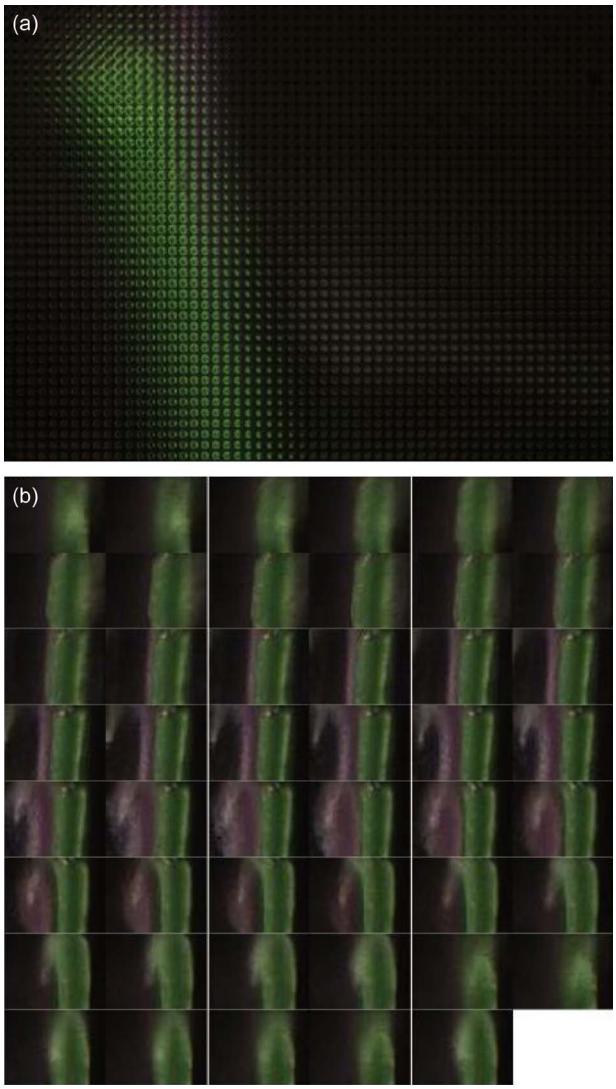

Fig. 6. Experimental results of camera B. (a) Captured lightfield of (green and purple) two wires placed along the same axis. (b) Smaller images show the digitally postprocessed images with 47 different viewpoints of the wires. The figure also shows the difference in image quality between the different viewpoints, whereas the images in the center (rows 4–6) are much sharper than the rest of the images. This difference in image quality is due to the nonuniform illumination of the pixels under each microlens where the central pixels will receive more uniform light compared to the pixels on the boundaries.

the angular resolution is determined by the number of pixels under each microlens [20]. If we want to increase the spatial resolution, we need to increase the number of microlenses. If the number of microlenses increases while using the same CCD imager, then the number of pixels under each microlens will decrease. This translates to a smaller number of available viewpoints.

B. Viewing Angle

The viewing angle of the micro camera is solely determined by the main lens focal length and size of the image plane. The viewing angle is given by the following equation:

$$\alpha = 2\tan^{-1}\left(\frac{d}{2i}\right) \tag{3}$$

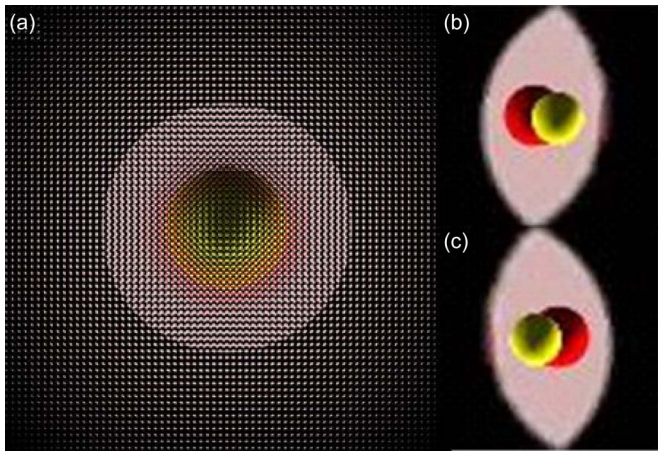

Fig. 7. Simulation result of a micro camera with a 2-mm aperture, f/4.5 main lens, and 69 $\times$ 69 50-μm-pitch microlenses. The scene is a yellow and a red object placed along the same axis. (a) Captured lightfield where only the yellow object can be seen because the red object is blocked by the yellow object. (b) and (c) show the digitally postprocessed images where the red object becomes visible from different angles.

where d is the horizontal size of the microlens array and i is the image distance. For camera A, d is fixed at 24.25 mm, and i was set at $\sim$68.5 mm, which results in an angle of $\alpha \sim 20^{\circ}$. For camera B, d is fixed at 4.6 mm, and i was set at $\sim$56 mm, which results in an angle of $\alpha \sim 4.7^{\circ}$. Note that the viewing angle values are not fixed since the image distance can be changed freely; these values just represent the results of our experimental conditions.

C. Microlens Aberrations

On the macroscale, optical aberrations in cameras are corrected by adding multiple lenses, thereby manipulating the optical path. This increase in optical path results in a much larger camera. In the context of micro cameras, we want to minimize aberrations as well as the optical path. When compared to macroscale camera lenses, a micro camera with a main lens that has the same f-number would have less aberration [21]. Efforts to digitally correct lens aberrations in macroscale lightfield cameras have also been established; however, they are targeted toward the main lens aberrations rather than the microlens array aberrations. Their algorithm requires the knowledge of the aberrations of the real lens used and then rearranges the light rays to where they should be in an ideal unaberrated case [22]. Others have suggested placing an aperture in front of each microlens to eliminate the effect of the aberrated lens edges [23]. These approaches, although possibly appropriate for macroscale cameras, are hard to implement for microscale cameras, if feasible at all. Our idea is to focus on minimizing aberrations by optimizing the choice of microlens array. Another reason to focus on the choice of microlens array is because the effective illumination of each pixel is determined by the microlens aberrations and diffraction.

There are different types of microlens arrays currently used, including the hexagonal, square, and circular. An important figure of merit used in determining the choice of microlens array is the fill factor. The fill factor is defined as the ratio of the area

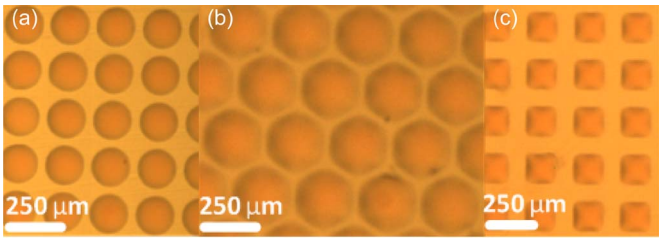

Fig. 8. Microlenses with different surface profiles fabricated by photoresist reflow method to test aberration. (a) Circular microlenses. (b) Hexagonal microlenses. (c) Square microlenses.

occupied by the lenses over the area of the overall array [17]. The higher the fill factor, the more efficient the microlens array is at collecting the incoming light. Circular microlenses have a maximum fill factor of 78.5% when arranged orthogonally and 90.6% when arranged in a honeycomb structure [24]. Both hexagonal and square microlenses have a fill factor of almost 100%. In terms of the micro camera, the fill factor affects the number of actual visible viewpoints that can be rendered. For example, in the case of camera B, the theoretical number of available viewpoints is 47 $\times$ 47; however, the actual number is less than that since there are some pixels that lie between the areas covered by neighboring microlenses. This can be seen in the rendered images in Fig. 6(b). If the choice of microlens array was based on fill factor alone, then it would seem trivial to choose either hexagonal or square microlens arrays. This leads to another important figure of merit used to determine the choice of microlens array which is microlens aberrations.

Since the footprints of these microlenses are different, the different shapes will have different aberration patterns. To study the aberrations, we fabricated additional hexagonal and square photoresist microlenses shown in Fig. 8, using the fabrication process described previously, to compare with the circular microlenses used in our micro cameras. The profiles of the lenses were then extracted using a white light interferometer (Zygo NewView 6300, Zygo Corporation, Middlefield, CT, USA), as shown in Fig. 9 [25]. In order to have a correct profile, the ZYGO requires the sample to be reflective so the microlenses were sputtered with approximately 10 nm of gold which does not alter the shape of the resulting profile. Although the ZYGO has built-in capabilities to measure the aberrations of the lens, they are only limited, however, to circular pupils which will not correctly reflect the aberrations of the hexagonal and square microlenses [26]. This is due to the fact that Zernike polynomials which are mathematical representations used to numerically characterize lens profiles are orthogonal over the unit circle only and not on other pupil shapes [27].

To correctly measure the aberrations of the hexagonal and square microlenses requires a different set of polynomials that are orthogonal over the respective pupils. These polynomials have been defined in terms of the Zernike circle polynomials. For the hexagonal lens, the polynomial representing spherical aberration is [27]

$$H = \frac{521}{\sqrt{1072205}}\boldsymbol{Z}_1 + 88\sqrt{\frac{15}{214441}}\boldsymbol{Z}_4 + 14\sqrt{\frac{43}{4987}}\boldsymbol{Z}_{11} \quad (4)$$

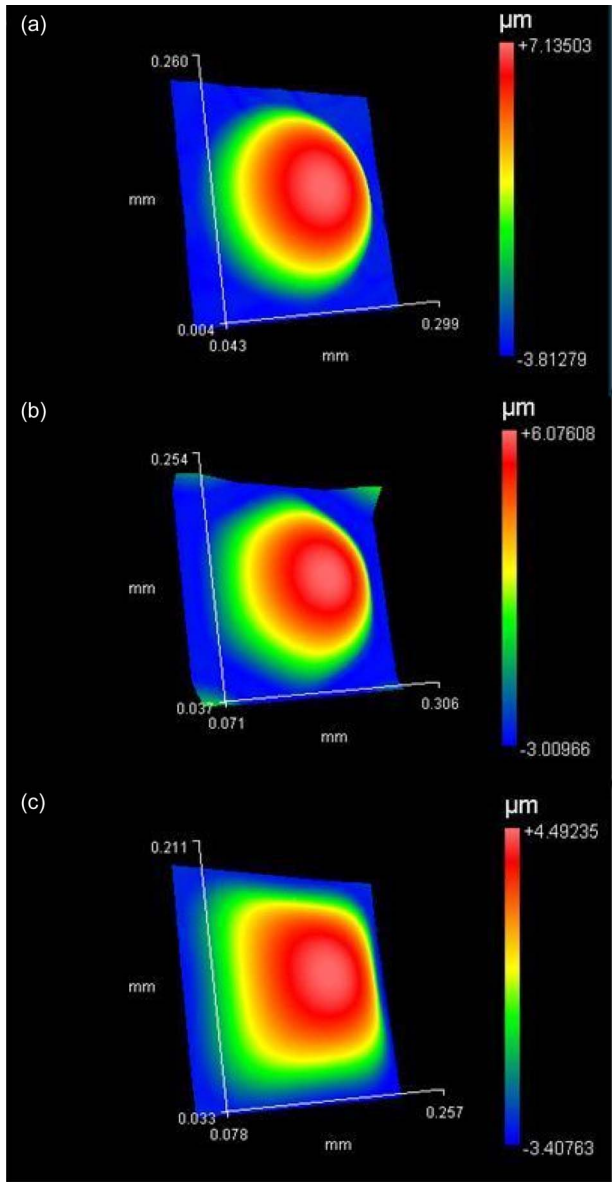

Fig. 9. Three-dimensional models of the photoresist microlenses provided by the white light interferometer. (a) Circular microlens with a height of 10.3 μm. (b) Hexagonal microlens with a height of 8.86 μm. (c) Square microlens with a height of 7.7 μm.

and for the square lens

$$S = \frac{8}{\sqrt{67}}\boldsymbol{Z}_1 + 25\frac{\sqrt{\frac{3}{67}}}{4}\boldsymbol{Z}_4 + 21\frac{\sqrt{\frac{5}{67}}}{4}\boldsymbol{Z}_{11} \quad (5)$$

$$\boldsymbol{Z_1} = 1 \quad (6)$$

$$\boldsymbol{Z_4} = \sqrt{3}(2\rho^2 - 1) \quad (7)$$

$$\boldsymbol{Z_{11}} = \sqrt{5}(6\rho^4 - 6\rho^2 + 1) \quad (8)$$

where $\mathbf{Z_1}$ is the circle orthonormal Zernike polynomial representing piston, $\mathbf{Z_4}$ represents defocus, $\mathbf{Z_{11}}$ represents primary spherical aberration, and ρ is the normalized radius [27].

To calculate the actual aberration, the resulting polynomial is then converted into an aberration in number of waves using the relation as follows [26]:

$$SA = 6Z \quad (9)$$

TABLE I
SPHERICAL ABERRATIONS OF MICROLENSES WITH DIFFERENT SURFACE PROFILES. SECOND COLUMN REPRESENTS THE DIAMETER OF THE CIRCULAR MICROLENS AND DIAGONAL OF THE SQUARE AND HEXAGONAL MICROLENSES, RESPECTIVELY

Comparison of spherical aberration of different lens profiles

Footprint	Size (μm)	f/#	Spherical aberration (wave)
Circle	230	4.5	1.58
Square	219	5.5	38.33
Hexagonal	220	4.9	34.91

where Z is the Zernike polynomial characterizing spherical aberration. Table I summarizes the results of the calculations. As can be seen from the table, both the photoresist hexagonal and square microlenses are highly aberrated.

Aside from the aberrations due to the shape of the lens, another source of aberration common to all the microlenses is the surface tension between the photoresist microlens and the underlying surface [23].

We are aware that the aforementioned aberrations do not reflect the minimal aberrations of some commercially available lenses. Nonetheless, they do reflect the trend of increasing aberrations between circular microlenses on one side and differently shaped microlenses on the other. We are also aware that such studies have been reported in [18], but we wanted to revisit this study in the context of our micro camera. Specifically, we studied the effect of the aforementioned aberrations on the resulting image quality by the use of the optical analysis software (Zemax SE, ZEMAX Development Corporation, Bellevue, WA, USA). In ZEMAX, we specifically used the image analysis tool which analyzes the resolution used to produce an image through the optical system [28]. We simulated an image of the letter F through the optical path of the micro camera and compared the images produced by one microlens. Fig. 10 shows the resulting image analysis spot diagrams when using a model microlens, circular, square, and hexagonal, respectively. The figures show relative similarities between the image plane spot diagrams. This shows that, even though the difference in aberrations of microlenses is significant, there is no significant difference in the overall image quality.

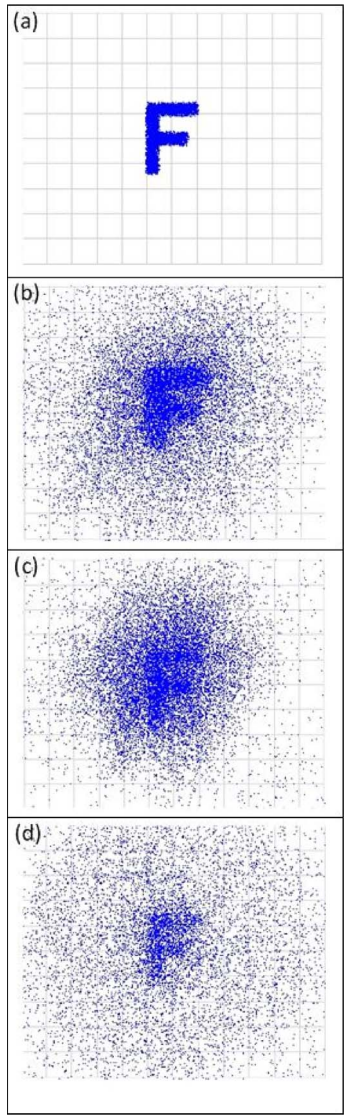

Fig. 10. ZEMAX image analysis of a camera setup. (a) Image analysis diagram of a model lens. The result shows no scattered light on the image plane. (b) Image analysis diagram of a circular microlens. Image clearly shows a letter F with aberrated scattered light. (c) Image analysis diagram of a hexagonal microlens. Image shows similar image to that in (b). (d) Image analysis diagram of a square microlens. Image shows relatively similar pattern to those from other microlenses.

VI. CONCLUSION

In summary, we have demonstrated micro cameras that provide multiple viewpoint imaging with only one exposure using a photoresist microlens array. The camera could potentially be used in any micro camera applications that suffer from limited maneuverability environments, such as endoscopic procedures. Optical aberrations of circular, square, and hexagonal microlenses have been determined by extracting the Zernike polynomials from the white light interferometer and orthogonalizing the Zernike polynomials for both hexagonal and square microlenses in terms of circular Zernike polynomials, as well as their effect on the image quality of lightfield photography. Square and hexagonal lenses suffered large aberrations as opposed to circular microlenses which suffered smaller aberrations. However, the aberrations had no significant effect on the quality of the captured image. Future work will involve placing the camera on a flexible curved surface to minimize aberrations and increase the field of view [29]. The cameras will be fabricated to even smaller dimensions and will also be integrated into complete optical systems such as endoscopes.

ACKNOWLEDGMENT

The authors would like to thank Prof. A. Sheinis and T. Portz for technical discussion and help. This research utilized NSF-supported shared facilities at the University of Wisconsin.

REFERENCES

[1] P. Breedveld, J. Sheltes, E. Blom, and J. Verheij, "A new, easily miniaturized steerable endoscope," *Eng. Med. Biol. Mag.*, vol. 24, no. 6, pp. 40–47, Nov./Dec. 2005.

[2] T. Adelson and J. Wang, "Single lens stereo with a plenoptic camera," *IEEE Trans. Pattern Anal. Mach. Intell.*, vol. 14, no. 2, pp. 99–106, Feb. 1992.

[3] M. Levoy and P. Hanrahan, "Light field rendering," in *Proc. 23rd Conf. Comput. Graph. Interactive Techn.*, New Orleans, LA, 1996, pp. 31–42.

[4] T. Georgiev and A. Lumsdaine, "Depth of field in plenoptic cameras," in *Proc. Eurographics*, Munich, Germany, 2009, pp. 5–8.

[5] G. Lippman, "La photographie integrale," *Comptes-Rendus, Académie des Sciences*, vol. 146, no. 9, pp. 446–451, 1908.

[6] R. Ng, M. Levoy, M. Brédif, G. Duval, M. Horowitz, and P. Hanrahan, "Light field photography with a hand-held plenoptic camera," Stanford Univ., Stanford, CA, Comput. Sci. Tech Rep. 2005-02, 2005.

[7] B. Wilburn, N. Joshi, V. Vaish, E. Talvala, E. Antunez, A. Barth, A. Adams, M. Horowitz, and M. Levoy, "High performance imaging using large camera arrays," *ACM Trans. Graph.*, vol. 24, no. 3, pp. 765–776, Jul. 2005.

[8] A. Veeraraghavan, R. Raskar, A. Agrawal, A. Mohan, and J. Tumblin, "Dappled photography: Mask enhanced cameras for heterodyned light field and coded aperture refocusing," *ACM Trans. Graph.*, vol. 26, no. 3, pp. 69-1–69-12, Jul. 2007.

[9] C. Chen, Y. Lu, and M. Su, "Light field based digital refocusing using a DSLR camera with a pinhole array mask," in *Proc. Int. Conf. Acoust., Speech, Signal Process.*, Dallas, TX, 2010, pp. 754–757.

[10] A. Levin, S. Hasinoff, P. Green, F. Durand, and W. Freeman, "4D frequency analysis of computational cameras for depth of field extension," *ACM Trans. Graph.*, vol. 28, no. 3, pp. 1–14, Aug. 2009.

[11] A. Lumsdaine and T. Georgiev, "The focused plenoptic camera," in *Proc. Int. Conf. Comput. Photogr.*, San Francisco, CA, 2009, pp. 1–8.

[12] Lytro. [Online]. Available: http://www.lytro.com/science_inside

[13] K. Fife, A. El Gamal, and H. Wong, "A multi-aperture image sensor with 0.7 μm pixels in 0.11 μm CMOS technology," *IEEE J. Solid State Circuits*, vol. 43, no. 12, pp. 2990–3005, Dec. 2008.

[14] A. Yaron, M. Shechterman, and N. Horesh, "Blur spot limitations in distal endoscope sensors," in *Proc. Stereoscopic Displays Virtual Reality Syst.*, San Jose, CA, 2006, pp. 78–84.

[15] B. Aldalali, C. Li, L. Zhang, and H. Jiang, "A micro camera utilizing a microlens array for multiple viewpoint imaging," in *Proc. 16th TRANSDUCERS*, Beijing, China, 2011, pp. 1582–1585.

[16] E. Adelson and J. Bergen, "The plenoptic function and the elements of early vision," in *Computational Models of Visual Processing*, M. Landy and J. Movshon, Eds. Cambridge, MA: MIT Press, 1991, pp. 3–20.

[17] H. Yang, C.-K. Chao, M.-K. Wei, and C.-P. Lin, "High fill-factor microlens array mold insert fabrication using a thermal reflow process," *J. Micromech. Microeng.*, vol. 14, no. 8, pp. 1197–1204, Aug. 2004.

[18] D. Daly, *Microlens Arrays*. New York: Taylor & Francis, 2001.

[19] S. Athineos, N. Sgouros, P. Papageorgas, D. Maroulis, M. Sangriotis, and N. Theofanous, "Photorealistic integral photography using a ray-traced model of capturing optics," *J. Electron. Imag.*, vol. 15, no. 4, p. 043007, Oct. 2006.

[20] T. Georgiev and A. Lumsdaine, "Resolution in plenoptic cameras," in *Proc. Comput. Opt. Sens. Imag.*, San Jose, CA, 2009.

[21] R. Völkel, M. Eisner, and K. J. Weible, "Miniaturized imaging systems," *Microelectron. Eng.*, vol. 67/68, pp. 461–472, Jun. 2003.

[22] R. Ng and P. Hanrahan, "Digital correction of lens aberrations in lightfield photography," in *Proc. Int. Opt. Des. Conf.*, Vancouver, BC, Canada, 2006, p. WB2.

[23] D. Lee and R. Haynes, "Characterization of lenslet arrays for astronomical spectroscopy," *Publ. Astron. Soc. Pacific*, vol. 113, no. 789, pp. 1406–1419, Nov. 2001.

[24] P. Naussbam, R. Völkel, H. P. Herzig, M. Eisner, and S. Haselbeck, "Design, fabrication and testing of microlens arrays for sensors and microsystems," *Pure Appl. Opt.*, vol. 6, no. 6, pp. 617–636, Nov. 1997.

[25] X. Zeng and H. Jiang, "PDMS microlens arrays fabricated through liquid phase photopolymerization and molding," *J. Microelectromech. Syst.*, vol. 17, no. 5, pp. 1210–1217, Oct. 2008.

[26] Zygo Corp. [Online]. Available: http://www.zygo.com

[27] M. Bass, V. Mahajan, and E. Van Stryland, *Handbook of Optics,* 3rd ed, vol. 2, *Design, Fabrication and Testing, Sources and Detectors, Radiometry and Photometry*. New York: McGraw-Hill, 2010.

[28] Zemax Corp. [Online]. Available: http://www.zemax.com

[29] B. Aldalali, D. Zhu, and H. Jiang, "Fabrication of polydimethylsiloxane microlens arrays on curved surfaces," in *Proc. Int. Conf. Opt. MEMS Nanophoton.*, Istanbul, Turkey, 2011, pp. 239–240.

Bader Aldalali received the B.S. degree from the School of Electrical and Computer Engineering, Purdue University, West Lafayette, IN, in 2005, and the M.S. degree in electrical engineering from the University of Wisconsin, Madison, in 2008, where he is currently working toward the Ph.D. degree in electrical engineering.

His research interests include lightfield cameras, optical microelectromechanical systems, and flexible electronics.

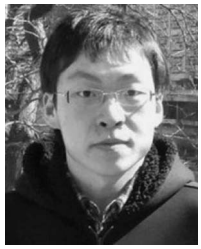

Chenhui Li received the B.S. degree in electrical engineering from Tsinghua University, Beijing, China, in 2007, and the M.S. degree in electrical and computer engineering from the University of Wisconsin, Madison, in 2010, where he is currently working toward the Ph.D. degree in electrical engineering.

His research interests include microoptical imaging, liquid focus-variable microlenses, electrowetting, and lightfield cameras.

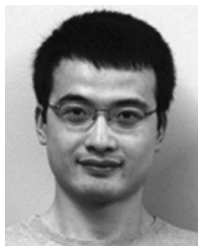

Li Zhang received the B.S. degree in automation from Tsinghua University, Beijing, China, and the M.S. and Ph.D. degrees in computer science and engineering from the University of Washington, Seattle, in 2001 and 2005, respectively.

From 2005 to 2007, he was a Postdoctoral Researcher with Columbia University, New York, NY. He is currently an Assistant Professor with the Department of Computer Sciences, a Faculty Affiliate with the Department of Electrical and Computer Engineering, and a member of the Eye Research Institute, University of Wisconsin, Madison. His research interests are in computer vision, graphics, and image processing.

Dr. Zhang was the recipient of a National Science Foundation Faculty Early Career Development Program (CAREER) Award in 2009, Alfred P. Sloan Research Fellowship in 2010, and Packard Fellowship for Science and Engineering in 2010.

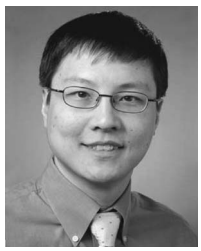

Hongrui Jiang (S'98–M'02–SM'10) received the B.S. degree in physics from Peking University, Beijing, China, in 1995, and the M.S. and Ph.D. degrees in electrical engineering from Cornell University, Ithaca, NY, in 1999 and 2001, respectively.

He is currently an Associate Professor with the Department of Electrical and Computer Engineering, a Faculty Affiliate with the Department of Biomedical Engineering, a Faculty Member of the Materials Science Program, and a Member of the Eye Research Institute, University of Wisconsin, Madison. From 2001 to 2002, he was a Postdoctoral Researcher with the Berkeley Sensor and Actuator Center, University of California, Berkeley. His research interests are in microfabrication technology, biological and chemical microsensors, microactuators, optical microelectromechanical systems, smart materials and micro-/nanostructures, lab-on-a-chip, and biomimetics and bioinspiration.

Dr. Jiang was the recipient of a National Science Foundation Faculty Early Career Development Program (CAREER) Award and Defense Advanced Research Project Agency Young Faculty Award in 2008, the H. I. Romnes Faculty Fellowship of the University of Wisconsin in 2011, and the National Institutes of Health (NIH) Director's New Innovator Award in 2011. He is currently a member of the Editorial Board of the JOURNAL OF MICROELECTROMECHANICAL SYSTEMS.